

Effects of Nb addition on structural evolution and properties of the $\text{CoFeNi}_2\text{V}_{0.5}$ high-entropy alloy

Li Jiang · Yiping Lu · Yong Dong ·
Tongmin Wang · Zhiqiang Cao · Tingju Li

Received: 14 October 2014 / Accepted: 21 December 2014 / Published online: 18 January 2015
© Springer-Verlag Berlin Heidelberg 2015

Abstract A series of $\text{CoFeNi}_2\text{V}_{0.5}\text{Nb}_x$ ($x = 0-1$) high-entropy alloys (HEAs) were synthesized to investigate the alloying effect of the Nb element on the microstructures and properties. It was found that the microstructures change from initial single-phase FCC solid solutions ($x = 0$), to a hypoeutectic microstructure ($0 < x < 0.75$), then to a fully eutectic microstructure ($x = 0.75$), and finally to a hypereutectic microstructure ($0.75 < x < 1$). The eutectic microstructure consists of the FCC solid solution phase and the Fe_2Nb -type Laves phase. Nb0 ($x = 0$) and Nb02 ($x = 0.2$) alloys exhibit excellent ductility, the compressive plastic elongation of which can reach up to 80 % without fracture. With increasing Nb content, increased brittle Laves phase leads to the decrease of the plastic strain and the increase of the yield strength, and the Vickers hardness shows an approximately linear increase from HV 133.4 to HV 687.7. Besides, the $\text{CoFeNi}_2\text{V}_{0.5}\text{Nb}_x$ HEAs exhibit excellent soft magnetic behavior, in which the Nb0 alloy shows the maximum saturation magnetization (M_s) of 70.33 emu/g, and minimum coercivity (H_c) of 1.62 Oe.

1 Introduction

In conventional alloy design, the materials are based on one or two principal elements with minor other alloying elements added to improve its properties. Recently, a new

type of alloys named as high-entropy alloys (HEAs) or multi-component equimolar or near-equimolar alloys has aroused great research interest [1–6]. These alloys are preferentially defined to compose of at least five principal elements each with a concentration ranging from 5 to 35 %. Multi-element effects as compared with conventional alloys endow HEAs with many effects, e.g., high-entropy, lattice distortion and sluggish diffusion effects [7]. The high-entropy effect lowers the free energy of the system which facilitates the formation of solid solution phase, particularly at high temperatures. The lattice distortion effect hinders dislocation movement and leads to pronounced solid solution strengthening. The sluggish diffusion effect stabilizes the alloy structure and increases the resistance to high-temperature softening [8–11]. As a result, the application of HEAs in high-temperature field is anticipated. The earliest high-temperature HEAs were reported by Senkov et al. [12–18], which was particularly relevant to aerospace industry. However, the poor room-temperature ductility limited these high-temperature HEAs for further processing steps. But the alloys with face-center-cubic (FCC) structure can own high plasticity and low stacking fault energy which contributes to the outstanding creep resistance [19, 20]. Hence, the researches on high-temperature HEAs with FCC structure become very significant. According to Guo et al.'s [21] theory, the FCC phase tends to form in HEAs with valence electron concentration (VEC) above 8. Therefore, much of high-temperature elements with high VEC are chosen to design the new alloy with FCC structure. Moreover, the vanadium element (V) possessing low density and excellent high-temperature performance [22, 23] has also been added to the new alloy. The niobium element (Nb) was often added to high-temperature alloys, such as in $\text{Fe}_2\text{V}_{1-x}\text{Nb}_x\text{Al}$ Heusler-type intermetallic alloys [24], and Inconel718

L. Jiang · Y. Lu (✉) · Y. Dong · T. Wang · Z. Cao (✉) · T. Li
School of Materials Science and Engineering, Dalian University
of Technology, Dalian 116024, China
e-mail: luyiping@dlut.edu.cn

Z. Cao
e-mail: caozq@dlut.edu.cn

superalloys [25]. In addition, the effect of Nb content on the magnetic properties was always a research hotspot [26, 27]. Thus, in this paper, a novel alloy system $\text{CoFeNi}_2\text{V}_{0.5}\text{Nb}_x$ with $\text{VEC} > 8$ (where x represents the atomic percentage ranging from 0 to 1) was designed and the variation of its microstructures as well as the mechanical and magnetic properties were investigated.

2 Experimental

The HEAs ingots with nominal composition of $\text{CoFeNi}_2\text{V}_{0.5}\text{Nb}_x$ (x value in molar ratio, $x = 0, 0.2, 0.4, 0.6, 0.65, 0.7, 0.75, 0.8$ and 1 denoted as Nb0, Nb02, Nb04, Nb06, Nb065, Nb07, Nb075, Nb08 and Nb1, respectively) were prepared using the vacuum arc melting method. The purity of the raw elemental metals is above 99.9 wt%. Approximately 35 g of the raw materials were melted in a water-cooled copper mold under an ultrahigh-purity argon (Ar) atmosphere. The ingots were flipped and remelted at least 5 times to improve chemical homogeneity.

The crystalline structures of the ingots were identified via X-ray diffractometry (XRD, EMPYREAN) with Cu-K_α radiation. The scanning range was from 20° to 100° , and the scanning rate was $0.215629^\circ/\text{s}$. Then, the samples were sectioned, grounded, polished and finally chemically etched with alcohol dilute aqua regia for observation under an optical microscope (MEF-3) and a field-emission-gun scanning electron microscope (Zeiss supra 55) equipped with the energy dispersive spectrometry (EDS). The volume fractions of different phases in the alloys were estimated using the Image-Pro Plus (IPP) software. The hardness values of the alloys were measured with a Vickers hardness tester (MH-50) under a load of 500 g and a holding time of 15 s. Measurements were made at least five points for each specimen with uniform distribution, and then, the average values were adopted in the paper. Compressive tests were performed on samples of $\Phi 5 \times 10$ mm using a testing machine (WPM) with a strain rate of $1 \times 10^{-3}/\text{s}$. The magnetization curves were measured with JDM-13T vibrating sample magnetometer.

3 Results and discussion

3.1 Crystal structure

Figure 1a shows the XRD patterns of the as-cast ingots with different Nb contents. Nb0 alloy exhibits a single FCC solid solution structure. With the addition of the Nb element, the microstructures of the Nb02–Nb1 alloys show a mixture of FCC solid solution phase and Fe_2Nb -type Laves phase with a hexagonal close-packed (HCP) lattice

structure. Furthermore, the total intensity of the Laves phase is evidently increasing with increasing Nb content, which even exceeds that of the FCC solid solution phase when x is above 0.8. Figure 1b shows the XRD peak shift of the (111) reflections for Nb0–Nb1 alloys. It is worth noting that the (111) peak initially shifts toward lower 2θ angle as $x \leq 0.6$, while toward higher 2θ as $x = 0.65, 0.7$ and then remains almost unchanged as $x \geq 0.7$. This change is consistent with the variation of the lattice constants of the FCC phase, which are calculated from the strongest (111) peak using the Bragg equation. The values of the lattice constants are 0.3567, 0.3593, 0.3603, 0.3614, 0.3613, 0.3607, 0.3607, 0.3608 and 0.3611 nm in the $\text{CoFeNi}_2\text{V}_{0.5}\text{Nb}_x$ alloys corresponding to $x = 0, 0.2, 0.4, 0.6, 0.65, 0.7, 0.75, 0.8$ and 1 , respectively. The solid solution of the Nb element with the largest atomic radius (see Table 1) can cause lattice distortion and thus increase the lattice constants. While the formation of a large amount of Fe_2Nb -type Laves phase will release the lattice distortion energy when the Nb element exceeds the solution limit, i.e., $x > 0.6$, as a result, the lattice constants decrease. The lattice strains can be expressed as $\varepsilon = \Delta a/a_0$, where $\Delta a = |a - a_0|$, by assuming $\text{CoFeNi}_2\text{V}_{0.5}$ as a “perfect” crystal. Figure 2 shows the tendency of the lattice strains with the increase of the Nb content. It can be seen that the lattice strains firstly increase ($x \leq 0.6$) and then decrease ($x > 0.6$), which also suggests that the solution limit of the Nb element into the FCC solid solution is no more than 11.76 at. % corresponding to $x = 0.6$.

3.2 Microstructure

To further investigate the microstructure transformation caused by the addition of Nb, the microstructures of the as-cast samples with different Nb contents are presented in Figs. 3 and 4. The columnar grain microstructure of the Nb0 alloy confirms its single-phase structure. Combined with the XRD results, a conclusion can be drawn that the Nb0 alloy consists of a single-phase FCC structure (see Figs. 1a, 3a). The Nb02 and Nb04 alloys show a typical dendritic morphology, and the dendritic phase (marked as A) is the FCC solid solution phase and the interdendritic section has an eutectic microstructure with a mixture of Fe_2Nb -type Laves phase and FCC solid solution phase, as shown in Fig. 3b, c. The Nb06, Nb065 and Nb07 alloys display similar morphologies, which exhibit a typical hypoeutectic structure, and the primary phase is the FCC solid solution phase (marked as A), as shown in Fig. 3d–f. The volume fractions of the eutectic microstructures are 40.3, 58.3, and 70 %, respectively for Nb06, Nb065 and Nb07 alloys, which indicates the volume fraction of the eutectic microstructure increases with increasing Nb content. The Nb075 alloy shows a fully eutectic microstructure, as presented in the

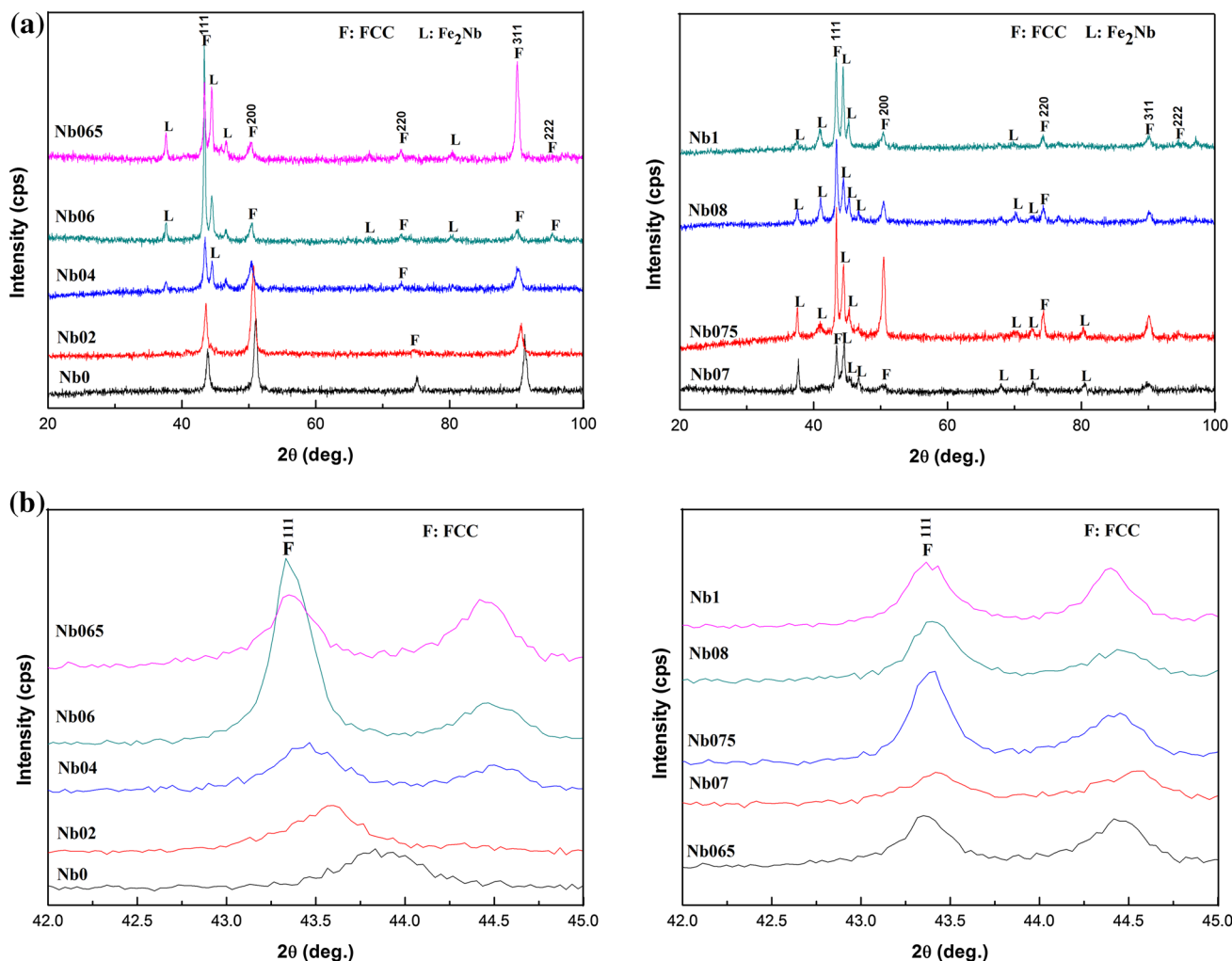


Fig. 1 **a** X-ray diffraction pattern of the as-cast CoFeNi₂V_{0.5}Nb_x ($x = 0-1$) HEAs, **b** shift of the (111) peaks corresponding to the major FCC phase

Table 1 The mixing enthalpy ΔH_{mix} (kJ/mol) of atom pairs; lattice parameter (\AA) of each element

a_i (\AA)	Co	Fe	Ni	V	Nb
	1.25	1.26	1.24	1.34	1.46
Co	–	–1	0	–14	–25
Fe	–	0	–2	–7	–16
Ni	–	–	0	–18	–30
V	–	–	–	0	–1
Nb	–	–	–	–	0

magnified pictures in Fig. 4f, g. Both the Nb08 and Nb1 alloys present a hypereutectic microstructure, the primary phase is the Laves phase, marked as B. And the volume fractions of the eutectic microstructure of Nb08 and Nb1 are 78.3 and 53.8 %, respectively. Similar results can be observed from the XRD analysis that the total intensity of

the Laves peaks increase with increasing Nb content, which is even higher than that of the FCC phase in the Nb08 and Nb1 alloys (see Fig. 1). To summarize, for the CoFeNi₂V_{0.5}Nb_x alloy system, with the addition of the Nb element, the microstructure changes from single-phase FCC solid solutions ($x = 0$), to a hypoeutectic microstructure ($0 < x < 0.75$), then to a fully eutectic microstructure ($x = 0.75$), and finally to a hypereutectic microstructure ($0.75 < x < 1$). The schematic phase diagram is shown in Fig. 5.

Table 2 summarizes the EDS results of different regions in the as-cast CoFeNi₂V_{0.5}Nb_x alloys. The Nb0 alloy exhibits relatively uniform elemental distribution. As for the Nb02–Nb07 alloys, the chemical composition of dark A region corresponding to the FCC phase is enriched with V and poor with Nb element, while the Co, Fe, Ni elements approximately match the nominal composition of the designed alloys. It was known that Co, Fe, Ni

Fig. 2 Lattice strains and Vickers hardness of the as-cast $\text{CoFeNi}_2\text{V}_{0.5}\text{Nb}_x$ HEAs with increasing Nb content

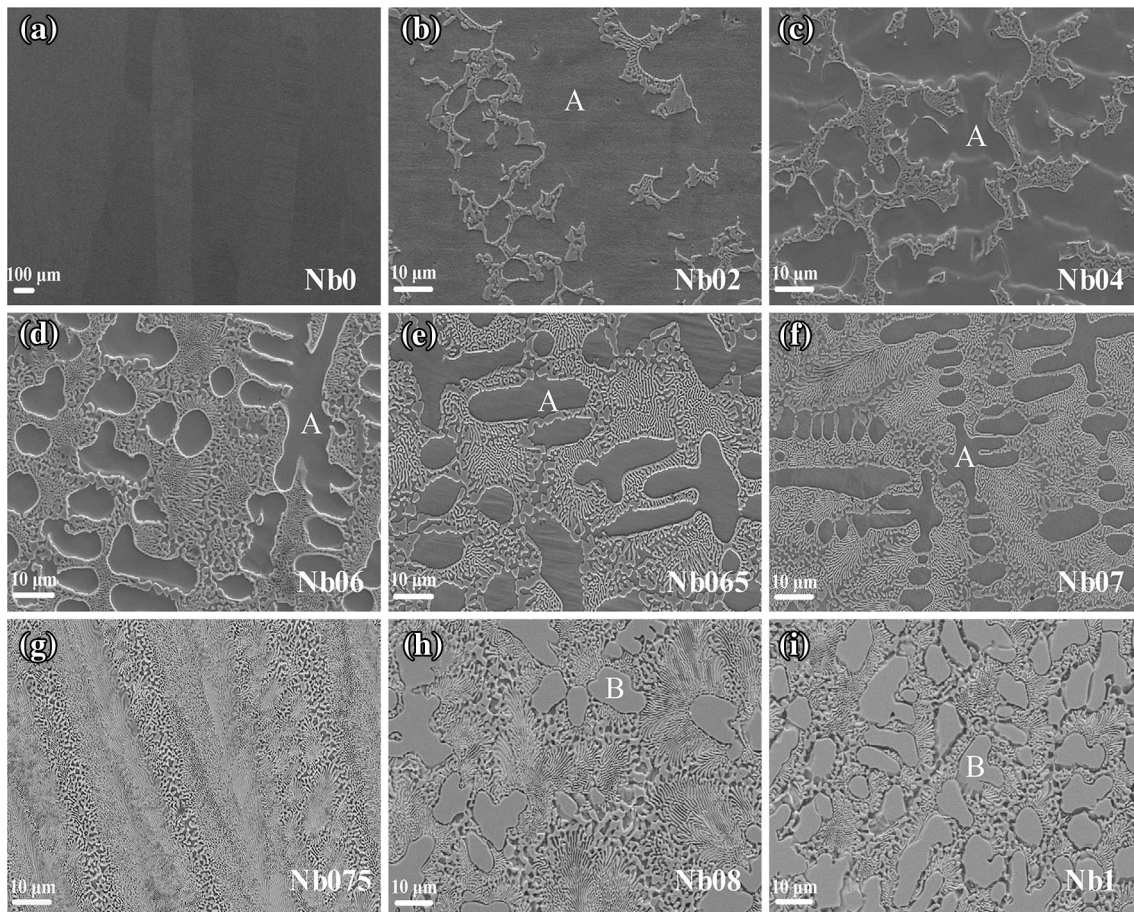
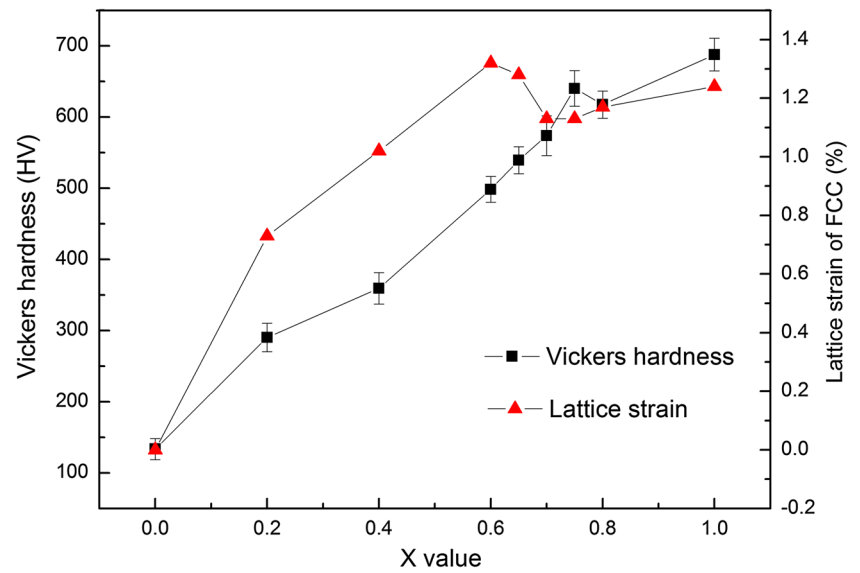


Fig. 3 Microstructures of the as-cast $\text{CoFeNi}_2\text{V}_{0.5}\text{Nb}_x$ HEAs, showing microstructural evolution from single-phase FCC structure (a) to dendritic microstructure (b, c), then to hypoeutectic microstructure

(d–f), then to eutectic microstructure (g), and finally to hypereutectic microstructure (h–i)

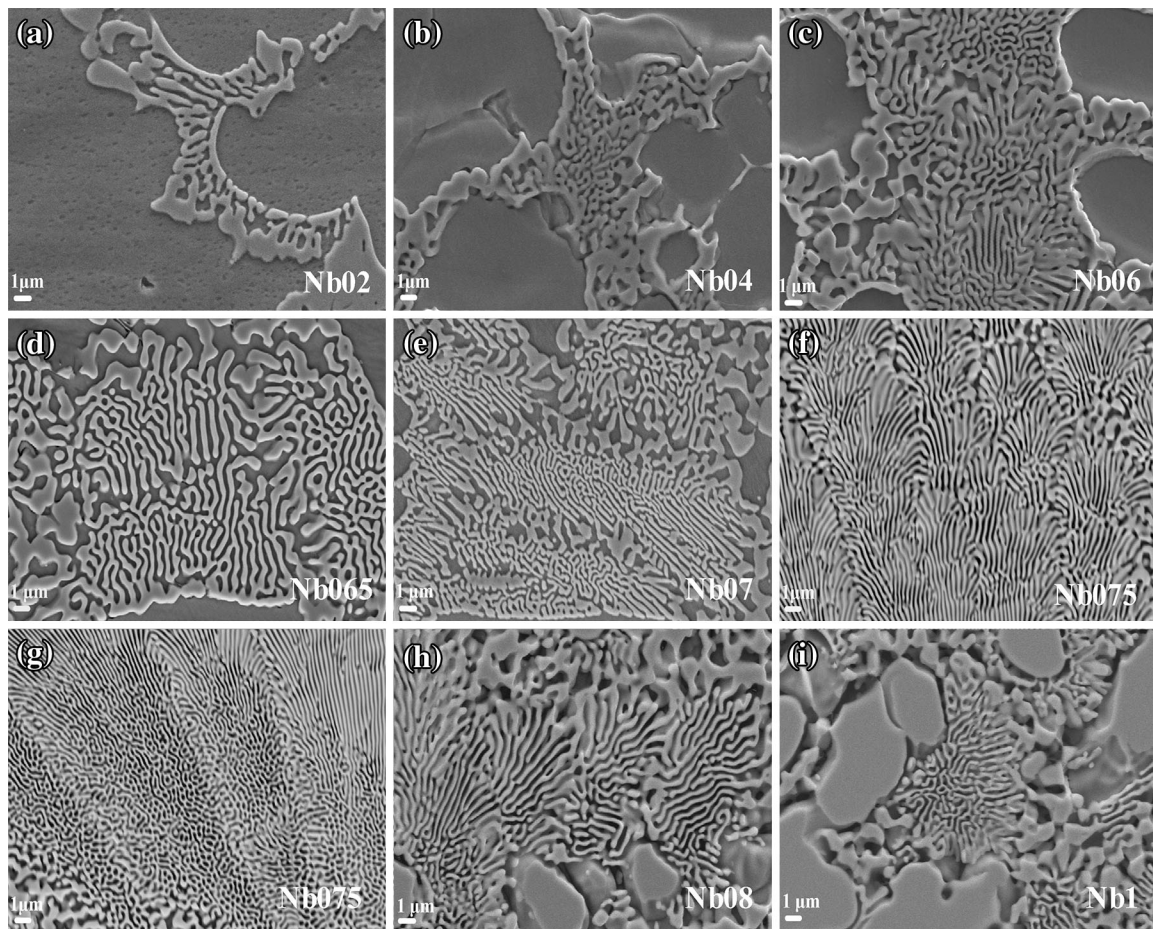


Fig. 4 Magnified SEM imagines of the eutectic regions of the $\text{CoFeNi}_2\text{V}_{0.5}\text{Nb}_x$ HEAs

elements are neighbors in periodic table of elements, their atomic sizes are similar, and their mixing enthalpy is close to zero (listed in Table 1). So these three elements tend to distribute uniformly in the alloys. While the bright B region corresponding to the Laves phase in Nb08 and Nb1 alloys is enriched with Nb element. This is because Nb element with large atomic size as well as negative mixing enthalpies with other alloying elements (see Table 1) is not favorable to solute into the FCC solid solution but tends to form the Laves phase. It is also found that the alloys consisting of two atomic groups with distinctively different mixing enthalpy tend to form the eutectic microstructure.

3.3 Mechanical properties

The Vickers hardness curve of the $\text{CoFeNi}_2\text{V}_{0.5}\text{Nb}_x$ alloys is plotted in Fig. 2. It was found that the Vickers hardness has an approximately linear increase from Nb0 to Nb1 alloys within the error. The linear line can be expressed as

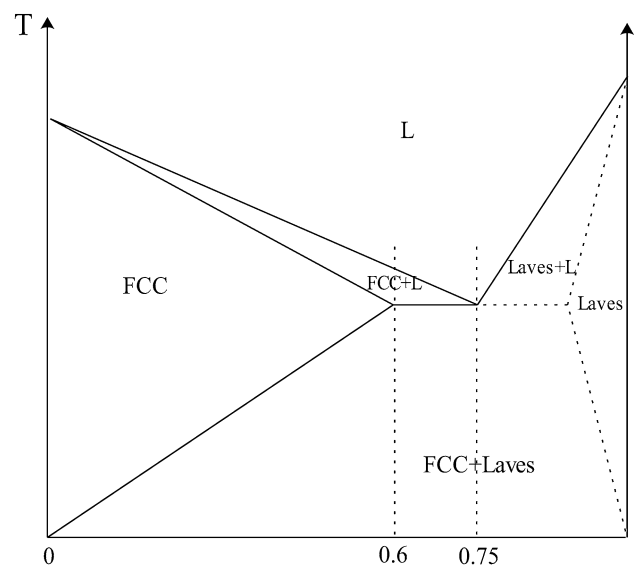
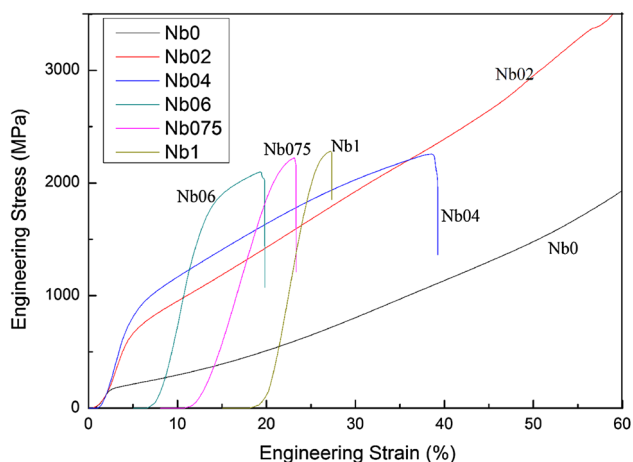


Fig. 5 A schematic phase diagram of the as-cast $\text{CoFeNi}_2\text{V}_{0.5}\text{Nb}_x$ HEAs

Table 2 Chemical compositions of different regions in the CoFe-Ni₂V_{0.5}Nb_x HEAs by EDS (at. %)

Alloys	Regions	Chemical compositions/at. %				
		Co	Fe	Ni	V	Nb
Nb0		22.2	21.8	45.0	11.0	–
Nb02	A	18.8	19.6	39.1	19.8	2.7
Nb04	A	19.8	21.4	41.0	11.5	6.3
Nb06	A	19.3	22.5	39.4	12.2	6.6
Nb065	A	19.2	22.1	39.4	11.7	7.7
Nb07	A	19.5	21.5	40.2	11.3	7.5
Nb075		20.9	17.4	30.0	4.9	26.8
Nb08	B	21.8	17.2	26.5	5.2	29.2
Nb1	B	19.0	19.5	26.8	5.5	29.1

**Fig. 6** Compressive engineering stress–strain curves of the representative hypoeutectic, eutectic and hypereutectic CoFeNi₂V_{0.5}Nb_x HEAs ($x = 0, 0.2, 0.4, 0.6, 0.75, 1$)**Table 3** Mechanical properties of the representative hypoeutectic, eutectic and hypereutectic CoFeNi₂V_{0.5}Nb_x HEAs ($x = 0, 0.2, 0.4, 0.6, 0.75, 1$)

Alloys	Yield stress σ_y (MPa)	Compressive strength σ_{max} (MPa)	Plastic strain ϵ_p (%)
Nb0	172	–	>80
Nb02	660	–	>80
Nb04	776	2,267	32.4
Nb06	1,806	2,101	7.8
Nb075	2,073	2,232	3.4
Nb1	2,108	2,280	2.5

$Y_{HV} = 605x + 133.4$, where Y_{HV} is the Vickers hardness and x is the Nb content.

The compressive engineering stress–strain curves of the representative hypoeutectic, eutectic and hypereutectic alloys are shown in Fig. 6. The yield strength (σ_y), fracture

strength (σ_{max}) and plastic strain (ϵ_p) are listed in Table 3. The compressive plastic elongation of the Nb0 and Nb02 alloys can reach up to 80 % without fracture. Especially for the Nb02 alloy, except for the excellent plasticity, it also owns a better yield strength of 660 MPa. Further increase of the Nb content causes increased brittle Laves phase, which leads to the decrease of the plastic strain and the increase of the yield strength.

3.4 Magnetic properties

Hysteresis loop measurement for the representative hypoeutectic, eutectic and hypereutectic CoFeNi₂V_{0.5}Nb_x alloys at room temperature are shown in Fig. 7. The saturation magnetization (M_s), remnant magnetism (M_r) and coercivity (H_c) of the alloys obtained from the loops are listed in Table 4. Another parameter χ is calculated using:

$$\chi = \frac{\sigma(\text{emu/g}) \cdot \rho(\text{g/cm}^3)}{4\pi \cdot H(\text{Oe})}$$

where χ is the permeability, H is the magnetic field intensity, σ is the specific saturation magnetization and ρ is the density of alloys. It can be seen, the χ values of the CoFeNi₂V_{0.5}Nb_x alloys can be calculated to be 1.17×10^{-2} to 6.9×10^{-4} , indicates its ferromagnetic behavior. With the increase of the paramagnetic Nb element, both M_s and χ decrease, which suggests a reduced ferromagnetic behavior. The low H_c values of the CoFeNi₂V_{0.5}Nb_x HEAs (1.62–43.32 Oe) reveal its soft magnetic behavior, but with increasing Nb content, H_c increase. This may be explained as that H_c is expected to be sensitive to the grain size, impurities and lattice distortion, the increasing Laves phase boundaries with increasing Nb content can strongly hinder the shift of domain-walls, which leads to the increase of H_c . The effect of the Nb element on the magnetic properties of present alloy system

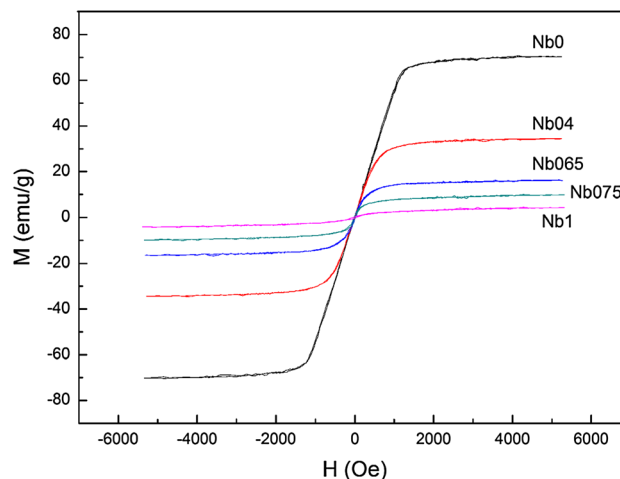
**Fig. 7** Magnetic curves of the representative hypoeutectic, eutectic and hypereutectic CoFeNi₂V_{0.5}Nb_x HEAs ($x = 0, 0.4, 0.65, 0.75, 1$)

Table 4 Magnetic properties of the representative hypoeutectic, eutectic and hypereutectic CoFeNi₂V_{0.5}Nb_x HEAs ($x = 0, 0.4, 0.65, 0.75, 1$)

Alloys	M_s , emu/g	M_r , emu/g	H_c , Oe	χ
Nb0	70.33	0.4750	1.62	11.7
Nb04	34.07	0.5084	5.87	5.67
Nb065	16.29	0.6870	14.38	2.7
Nb075	9.74	0.8721	19.38	1.6
Nb1	4.16	0.7780	43.32	0.69

is identical to Ref. [28], in which both M_s and M_r decreased, while H_c increased with increasing Nb content.

4 Conclusions

The CoFeNi₂V_{0.5}Nb_x (x value in molar ratio, $x = 0, 0.2, 0.4, 0.6, 0.65, 0.7, 0.75, 0.8$ and 1) HEAs were produced by vacuum arc melting. Thereinto, the Nb0 alloy exhibits a single-phase FCC solid solution structure, whereas the Nb02–Nb1 alloys consist of FCC solid solution phase and Fe₂Nb-type Laves phase. Furthermore, a schematic phase diagram has been plotted to demonstrate the change of the microstructure, i.e., from single-phase FCC solid solutions ($x = 0$), to a hypoeutectic microstructure ($0 < x < 0.75$), then to a fully eutectic microstructure ($x = 0.75$), and finally to a hypereutectic microstructure ($0.75 < x < 1$). With the increase of the Nb content from $x = 0$ to 1.0 , the compressive yield strength increases from 172 to 2,108 MPa, the hardness increases from HV133.4 to HV687.7, and the plastic strain decreases from above 80 to 2.5 %. Excellent soft magnetic behavior has also been observed in CoFeNi₂V_{0.5}Nb_x HEAs when $0 < x < 1$.

Acknowledgments This work was supported by the National Natural Science Foundation of China Nos (51134013, 51075070, 51104029 and 313011), respectively, the natural science foundation of Liaoning Province (2014028013) and the fundamental research funds for the central universities.

References

1. B. Cantor, I.T.H. Chang, P. Knight, A.J.B. Vincent, *Mater. Sci. Eng. A* **375–377**, 213–218 (2004)

2. J.W. Yeh, S.K. Chen, S.J. Lin, J.Y. Gan, T.S. Chin, T.T. Shun, C.H. Tsau, S.Y. Chang, *Adv. Eng. Mater.* **6**, 299–303 (2004)
3. Y. Zhang, T.T. Zuo, Z. Tang, M.C. Gao, K.A. Dahmen, P.K. Liaw, Z.P. Lu, *Prog. Mater. Sci.* **61**, 1–93 (2014)
4. B. Gludovatz, A. Hohenwarter, D. Catoor, E.H. Chang, E.P. George, R.O. Ritchie, *Science* **345**, 1153–1158 (2014)
5. P. Koželj, S. Vrtnik, A. Jelen, S. Jazbec, Z. Jagličić, S. Maiti, M. Feuerbacher, W. Steurer, J. Dolinšek, *Phys. Rev. Lett.* **113**, 107001-1–107001-5 (2014)
6. Y.P. Lu, Y. Dong, S. Guo, L. Jiang, H.J. Kang, T.M. Wang, B. Wen, Z.J. Wang, J.C. Jie, Z.Q. Cao, H. Ruan, T.J. Li, *Sci. Rep.* **4**, 6200-1–6200-5 (2014)
7. M. Tsai, J. Yeh, *Mater. Res. Lett.* **2**, 107–123 (2014)
8. C. Juan, C. Hsu, C. Tsai, W. Wang, T. Sheu, J. Yeh, S. Chen, *Intermetallics* **32**, 401–407 (2013)
9. C. Hsu, C. Juan, W. Wang, T. Sheu, J.W. Yeh, S. Chen, *Mater. Sci. Eng. A* **528**, 3581–3588 (2011)
10. H. Zhang, Y. He, Y. Pan, S. Guo, *J. Alloy Compd.* **600**, 210–214 (2014)
11. W. Wang, W. Wang, J.W. Yeh, *J. Alloy Compd.* **589**, 143–152 (2014)
12. O.N. Senkov, S.V. Senkova, D.M. Dimiduk, C. Woodward, D.B. Miracle, *J. Mater. Sci.* **47**, 6522–6534 (2012)
13. O.N. Senkov, J.M. Scott, S.V. Senkova, F. Meisenkothen, D.B. Miracle, C.F. Woodward, *J. Mater. Sci.* **47**, 4062–4074 (2012)
14. O.N. Senkov, J.M. Scott, S.V. Senkova, D.B. Miracle, C.F. Woodward, *J. Alloy Compd.* **509**, 6043–6048 (2011)
15. O.N. Senkov, G.B. Wilks, J.M. Scott, D.B. Miracle, *Intermetallics* **19**, 698–706 (2011)
16. O.N. Senkov, S.V. Senkova, C. Woodward, D.B. Miracle, *Acta Mater.* **61**, 1545–1557 (2013)
17. O.N. Senkov, C.F. Woodward, *Mater. Sci. Eng. A* **529**, 311–320 (2011)
18. O.N. Senkov, S.V. Senkova, D.B. Miracle, C. Woodward, *Mater. Sci. Eng. A* **565**, 51–62 (2013)
19. J.Y. He, C. Zhu, D.Q. Zhou, W.H. Liu, T.G. Nieh, Z.P. Lu, *Intermetallics* **55**, 9–14 (2014)
20. A.J. Zaddach, C. Niu, C.C. Koch, D.L. Irving, *JOM* **65**, 1780–1789 (2013)
21. S. Guo, C. Ng, J. Lu, C.T. Liu, *J. Appl. Phys.* **109**, 103505 (2011)
22. F. Tian, L.K. Varga, N. Chen, J. Shen, L. Vitos, *J. Alloy Compd.* **599**, 19–25 (2014)
23. C. Li, X. Mi, W. Ye, S. Hui, Y. Yu, W. Wang, *Mater. Sci. Eng. A* **578**, 103–109 (2013)
24. R. Saha, V. Srinivas, T.V. Chandrasekhar, Rao, A. Banerjee, *J. Magn. Magn. Mater.* **324**, 1071–1079 (2012)
25. C.F. Yao, Q.C. Jin, X.C. Huang, D.X. Wu, J.X. Ren, D.H. Zhang, *Int. J. Adv. Manuf. Technol.* **65**, 1019–1030 (2013)
26. J. Wang, Z. Zheng, J. Xu, Y. Wang, *J. Magn. Magn. Mater.* **355**, 58–64 (2014)
27. L.H. Kong, Y.L. Gao, T.T. Song, Q.J. Zhai, *J. Magn. Magn. Mater.* **323**, 2165–2169 (2011)
28. S.G. Ma, Y. Zhang, *Mater. Sci. Eng. A* **532**, 480–486 (2012)